MULTIFRAME NONRIGID MOTION ANALYSIS WITH ANISOTROPIC SPATIAL CONSTRAINTS: APPLICATIONS TO CARDIAC IMAGE ANALYSIS *

Ken Wong[1], *Huafeng Liu*[1,2], *Albert Sinusas*[3], *and Pengcheng Shi*[1]

[1] Medical Image Computing Group, Department of Electrical and Electronic Engineering
Hong Kong University of Science and Technology, Clear Water Bay, Kowloon, Hong Kong
[2] State Key Laboratory of Modern Optical Instrumentation, Zhejiang University, Hangzhou, China
[3] Section of Cardiology, Departments of Diagnostic Radiology and Medicine
Yale University School of Medicine, New Haven, CT 06520, USA

ABSTRACT

Proper spatial and temporal constraints are essential for image-based motion recovery of deforming objects. Since biological organs, such as the heart, are typically composed of fibrous tissues of anisotropic nature, one must adopt realistic spatial models, in addition to those important considerations for temporal modeling, in order to properly regularize the object behavior for kinematics recovery. We present a biomechanically-constrained state space analysis framework for the multiframe estimation of the heart motion and deformation. While the anisotropic physical constraints enforce spatial regulations on the myocardial behavior and spatial filtering of the image data measurements, statistical filtering techniques impose temporal constraints to incorporate multiframe information. Implemented within a meshfree particle representation and computation framework, excellent experimental results are achieved for both synthetic data with known ground truth and canine magnetic resonance image sequences with known clinical gold standard.

1. INTRODUCTION

Nonrigid motion analysis has significant implications for understanding the intrinsic behaviors of natural objects, such as the cardiac dynamics from tomographic medical image sequences. While there have been proven evidences from invasive procedures that the heart geometry and kinematics are of extreme complexity, current imaging data typically only provide noisy cardiac motion measurements on a sparse set of salient landmark points, such as the Lagrangian tag displacements from the magnetic resonance (MR) tagging images and the Eulerian tissue velocities from the MR phase contrast or Doppler echocardiographic data. In order to obtain the dense field motion which more completely assesses the overall and localized cardiac state of health, proper *a priori* spatial and temporal constraints are needed for the unique solution in some optimal sense [3].

To constrain the spatial relationship between the sparse feature points, a variety of strategies have been proposed for the cardiac image analysis, including the mathematical and statistical regularization models such as local smoothness [11] and spatial kriging model [7]. More recently, continuum biomechanics constraints have become increasingly popular because of the physical meaningfulness of these models [13, 14]. Nevertheless, most efforts have been relying on the simple, and grossly unrealistic, isotropic material models of the heart muscle. Anatomically, however, about 70% of the myocardial volume is occupied by the myocytes that are connected together by collagenous networks [5]. They are further bundled together to form the myofiber structure, where the elasticity properties along and cross the fibers are substantially different [4]. Thus, anisotropic material models must be adopted in order to properly constrain the myocardial behavior for a realistic nonrigid motion recovery.

Temporal constraints are also of paramount importance for cardiac image analysis. While most of the existing efforts, especially those relying on biomechanics-based spatial constraints, have concentrated on frame-to-frame analysis without explicit temporal models to enforce multiframe consistency [3], several works do attempt to alleviate the noise problems of the landmark data and to make use of the periodic nature of the cardiac motion by using either the minimum mean-square-error criteria under Gaussian assumptions [7, 8, 11] or the robust minimum maximum-error criterion [9] with notably improved results.

We have recently demonstrated the importance of adopting the anisotropic spatial models for the frame-to-frame motion estimation, especially with the meshfree particle framework which offers substantial advantages in handling myofiber orientations, geometry and kinematics discontinuities, and representation refinement [15]. In this paper, we further incorporate the temporal models of the heart motion to allow multiframe analysis with our anisotropic biomechanically-constrained state space framework. In addition to synthetic simulation results which exhibit superior performance over existing strategies, experiments with canine MR image sequences have produced physiologically sensible outcomes.

2. METHODOLOGY

2.1. Meshfree Particle Representation

With the meshfree particle method (MPM) [8], the left ventricle of the heart is represented by a set of unstructured, adaptively sampled nodal points, bounded by the segmented endocardium and epicardium. The first image at the bottom of Fig.1 shows a two-dimensional myocardial slice using the MPM representation. The density of the nodal distribution can be refined through node addition and removal, depending on the available computational re-

*THIS WORK IS SUPPORTED IN PART BY HKRGC GRANT HKUST6151/03E, BY NATIONAL BASIC RESEARCH PROGRAM OF CHINA NO: 2003CB716104, AND BY NIH GRANT R01HL065662.

0-7803-8554-3/04/$20.00 ©2004 IEEE.

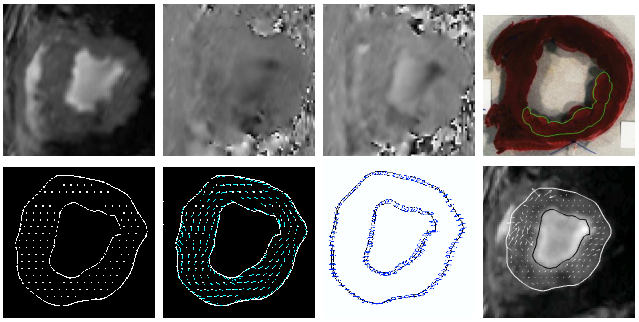

Fig. 1. Top: MR intensity, x-direction velocity, y-direction velocity images of frame #9, and the TTC-stained post mortem myocardium with infarcted tissue highlighted (left to right). Bottom: meshfree representation of the left ventricle, myofiber orientations, boundary displacement constraints, and phase contrast velocity map (left to right).

sources and the required precision. Further, it has been shown that MPM offers much improved accuracy and convenience in handling anisotropic orientations, tissue discontinuities, and *h-p* adaptations [15].

Analogous to the popular finite element methods (FEM), the field variable (i.e. the displacement vector in motion analysis) of the MPM represented object is constructed using the moving-least squares (MLS) approximation [8]. Let $u(\mathbf{x})$ be the displacement function of the myocardial tissue at $\mathbf{x}$, the approximated displacement function $u^h(\mathbf{x})$ is then computed from

$$u^h(\mathbf{x}) = \sum_{I=1}^{n}\sum_{j=1}^{m} p_j(\mathbf{x})(\mathbf{A}^{-1}(\mathbf{x})\mathbf{B}(\mathbf{x}))_{jI}u_I \equiv \sum_{I}^{n}\phi_I(\mathbf{x})u_I, \quad (1)$$

where

$$\mathbf{A}(\mathbf{x}) = \textstyle\sum_{I=1}^{n} w_I(\mathbf{x})\mathbf{p}(\mathbf{x}_I)\mathbf{p}^T(\mathbf{x}_I), w_I(\mathbf{x}) \equiv w(\mathbf{x}-\mathbf{x}_I)$$
$$\mathbf{B}(\mathbf{x}) = [w_1(\mathbf{x})\mathbf{p}(\mathbf{x}_1), w_2(\mathbf{x})\mathbf{p}(\mathbf{x}_2), ..., w_n(\mathbf{x})\mathbf{p}(\mathbf{x}_n)]$$
$$\mathbf{u}^T = [u_1, u_2, ...u_n]$$

with n the total number of sampling nodes, x_I the nodal coordinates, u_I the nodal displacement values, and m the number of terms in the basis $\mathbf{p}(\mathbf{x})$. Further, in these equations, the weight function $w_I(\mathbf{x})$ defines the local proximity and nodal connectivity between different nodes.

2.2. Anisotropic Composite Material Model

As discussed earlier, realistic anisotropic material models are essential for the accurate recovery of cardiac movement. In general, a mixture of two or more distinct material constituents or phases is called a *composite* [10]. For myocardium, the collagen tissues (the continuous constituent, or the *matrix*) is reinforced by the muscle fibers (the *reinforcement* tissues). Since the Young's moduli for a composite material with fibrous reinforcements are different along and cross the fibers, the myocardium is anisotropic in nature. Mechanical testings have shown that the material properties of the transverse planes along the myofiber is nearly isotropic [4], the myofibers are thus modeled as transversely isotropic materials in our work. Note, however, that fiber orientations are spatially varying from -60^o at the epicardium to $+60^o$ at the endocardium [12], the stress-strain relations at different locations of the heart are hence different under the same global coordinate system.

Material stiffness matrix for anisotropic myocardium: For both isotropic and anisotropic (transversely isotropic in our case) materials, the 2D stress-strain relationships obey the Hooke's Law:

$$\begin{bmatrix} S_{11} \\ S_{22} \\ S_{12} \end{bmatrix} = C \begin{bmatrix} \epsilon_{11} \\ \epsilon_{22} \\ \epsilon_{12} \end{bmatrix}, \quad (2)$$

where ϵ_{ij} are the components of the Green-Lagrangian strain tensor, S_{ij} are the components of the second Piola-Kirchhoff (PKII) stress tensor, and C is the stiffness matrix. Let the 2D stiffness matrix of a point with 0^o fiber orientation be C_o and of the form:

$$C_o = \begin{bmatrix} 1/E_f & -v/E_f & 0 \\ -v/E_f & 1/E_{cf} & 0 \\ 0 & 0 & 1/G \end{bmatrix}^{-1}, \quad (3)$$

where E_{cf} and E_f are the cross fiber and along fiber Young's modulus respectively, v is the Poisson ratio measuring the material compressibility (typically set to just under 0.5 for myocardium), and $G \approx E_f/(2(1+v))$ describes the shearing properties. Then, the stiffness matrix at any point with fiber orientation θ can be calculated from C_o through:

$$C_\theta = T^{-1}C_o R T R^{-1}. \quad (4)$$

where T is the coordinate transformation matrix:

$$T = \begin{bmatrix} \cos^2\theta & \sin^2\theta & 2\cos\theta\sin\theta \\ \sin^2\theta & \cos^2\theta & -2\cos\theta\sin\theta \\ -\cos\theta\sin\theta & \cos\theta\sin\theta & (\cos^2\theta - \sin^2\theta) \end{bmatrix} \quad (5)$$

and R is a matrix responsible for the transformation between the strain tensor components and the engineering strain tensor components:

$$R = \begin{bmatrix} 1 & 0 & 0 \\ 0 & 1 & 0 \\ 0 & 0 & 2 \end{bmatrix}. \quad (6)$$

2.3. Biomechanics-Based Myocardial System Dynamics

Once the anisotropic material model of the myocardium is determined, the system dynamic equations of the myocardium can be constructed with minimum potential principles [14].

Assuming infinitesimal deformation, i.e. using linearized Green-Lagrangian strain energy function $\epsilon_{ij} = \frac{1}{2}(u_{i,j}+u_{j,i})$ with $u_{i,j} = \partial u_i/\partial x_j$ at any point $\mathbf{x}$, the system dynamics with the MPM representation and the anisotropic material model becomes:

$$\mathbf{M}\ddot{\mathbf{u}} + \mathbf{C}\dot{\mathbf{u}} + [\mathbf{K} + \mathbf{K}^b]\mathbf{u} = \mathbf{R} + \mathbf{R}^b, \quad (7)$$

where $\dot{\mathbf{u}}$ and $\ddot{\mathbf{u}}$ are the first and second derivatives of $\mathbf{u}$ with respect to time, $\mathbf{M}$ is the mass matrix, $\mathbf{C}$ is the damping matrix, $\mathbf{K}$ is the stiffness matrix, $\mathbf{K}^b$ is the boundary condition penalty matrix, $\mathbf{R}$ is the external force, and $\mathbf{R}^b$ is the boundary condition force:

$$\mathbf{M}_{I,J} = \textstyle\int_\Omega \rho\Phi_I^T\Phi_J d\Omega,$$
$$\mathbf{K}_{I,J} = \textstyle\int_\Omega B_I^T C_\theta B_J d\Omega,$$
$$\mathbf{K}^b_{I,J} = \textstyle\int_{\Gamma_u} \Phi_I^T\alpha\Phi_J d\Gamma_u,$$
$$\mathbf{C}_{I,J} = \lambda_1\mathbf{M}_{I,J} + \lambda_2\mathbf{K}_{I,J} \text{ (Rayleigh Damping)},$$
$$\mathbf{R}^b_I = \textstyle\int_{\Gamma_u} \Phi_I^T\alpha\bar{\mathbf{u}}d\Gamma_u,$$
$$\Phi_I = \begin{bmatrix} \phi_I & 0 \\ 0 & \phi_I \end{bmatrix}, B_I = \begin{bmatrix} \phi_{I,x} & 0 \\ 0 & \phi_{I,y} \\ \phi_{I,y} & \phi_{I,x} \end{bmatrix},$$

with tissue density ρ, the penalty factor α, the shape function matrix Φ_I, and the strain matrix B_I at the I^{th} node. $\phi_{I,x}$ and $\phi_{I,y}$ are the derivatives of ϕ_I with respect to x and y, $\overline{\mathbf{u}}$ is the boundary displacement vector, Ω is the problem domain, and Γ_u is the essential boundary domain.

2.4. State Space Representation of System Dynamics

The system dynamics equation (7) can be converted into state space representation:

$$\dot{x}(t) = A_c x(t) + B_c w(t), \tag{8}$$

where

$$x(t) = \begin{bmatrix} \mathbf{u}(t) \\ \dot{\mathbf{u}}(t) \end{bmatrix}, \; w(t) = \begin{bmatrix} 0 \\ \hat{\mathbf{R}}(t) \end{bmatrix},$$
$$A_c = \begin{bmatrix} 0 & I \\ -\mathbf{M}^{-1}\hat{\mathbf{K}} & -\mathbf{M}^{-1}\mathbf{C} \end{bmatrix}, \; B_c = \begin{bmatrix} 0 & 0 \\ 0 & \mathbf{M}^{-1} \end{bmatrix},$$
$$\hat{\mathbf{R}} = \mathbf{R} + \mathbf{R}^b, \hat{\mathbf{K}} = \mathbf{K} + \mathbf{K}^b.$$

Assuming hidden Markov condition in time [1], including the zero-mean, additive, and white process noise $v(t)$ ($E[v(t)] = 0$, $E[v(t)v(s)'] = Q_v(t)\delta_{ts}$), equation (8) can be discretized into:

$$x(t+1) = Ax(t) + Bw(t) + v(t), \tag{9}$$

where $A = e^{A_c \Delta t}$, $B = A_c^{-1}(A - I)B_c$.

Since the data observations $y(t)$ obtained from the image are corrupted by noise, assuming zero-mean, additive, and white observation error $e(t)$ ($E[e(t)] = 0$, $E[e(t)e(s)'] = R_e(t)\delta_{ts}$), the measurement equation thus is:

$$y(t) = Hx(t) + e(t), \tag{10}$$

where H is a known, data-dependent measurement matrix.

2.5. Optimal Multiframe Kinematics Estimation

With the discretized state space equations (9,10), the multiframe estimation of the cardiac kinematics over the cardiac cycle can be performed using standard recursive Kalman filtering procedures until convergence [6] [1]:

1. Initial state and error covariance estimates, $\hat{x}(t-1)$ and $P(t-1)$.
2. Prediction step: using the update equations to predict the state and error covariance at time t:

$$\hat{x}^-(t) = A\hat{x}(t-1) + Bw(t), \tag{11}$$
$$P^-(t) = AP(t-1)A^T + Q_v(t). \tag{12}$$

3. Correction step: with the use of Kalman gain $G(t)$, the predictions are updated using the measurements $y(t)$:

$$G(t) = P^-(t)H^T(HP^-(t)H^T + R_e(t))^{-1}, \tag{13}$$
$$\hat{x}(t) = \hat{x}^-(t) + G(t)(y(t) - H\hat{x}^-(t)), \tag{14}$$
$$P(t) = (I - G(t)H)P^-(t). \tag{15}$$

[1] Relaxing the Gaussian assumptions on the system and data, robust H_∞ scheme can also be applied to perform the estimation [9].

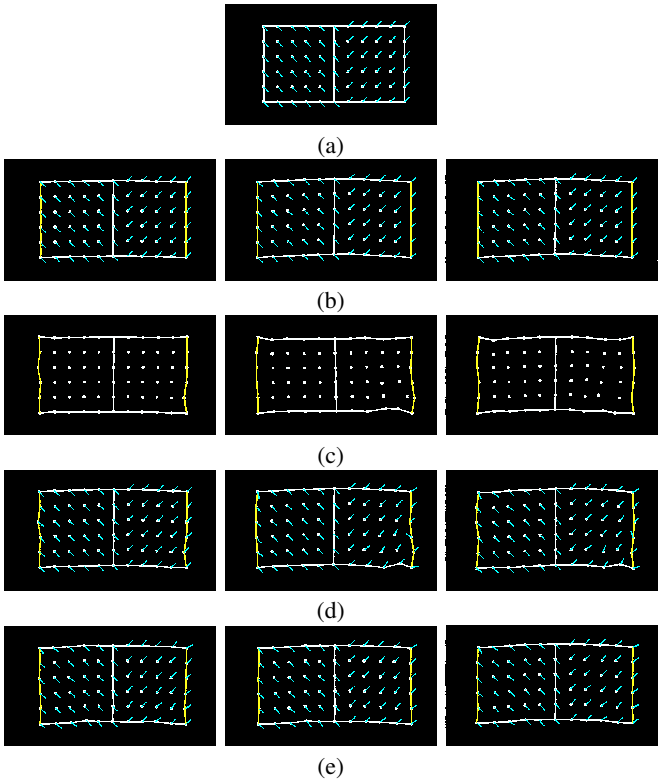

Fig. 2. Experiments on synthetic data. (a): Elastic object consists of two materials, with the short lines indicating the respective fiber orientations. (b): Three deforming frames (#2, #4, #6) of the object (out of six), generated by enforcing outward boundary displacements on the left and right edges. (c) to (e) are recovered object geometry from the noisy observations using: frame-to-frame estimation with isotropic material (c), frame-to-frame estimation with anisotropic material (d), and multiframe estimation with anisotropic material (e).

3. EXPERIMENTS

3.1. Synthetic Data

In order to show the importance of applying realistic anisotropic material models in a multiframe estimation fashion, experiments on synthetic data with known ground truth have been performed. A deformable rectangular object with two types of materials has been used to generate a sequence of 6 deforming frames, and the noise-corrupted displacements on the left and right edges are used as the data inputs for the experiments (see Fig.2). The importance of adopting proper spatial models and performing multiframe estimation is illustrated in our experiments. Comparing Fig.2(c) to Fig.2(d) and (e), it is obvious that the realistic anisotropic model has produced results much closer to the ground truth of Fig.2(b). Further, the multiframe estimation result of Fig.2(e) is greatly improved from its frame-to-frame counter parts (Fig.2(d)) with much better local coherence.

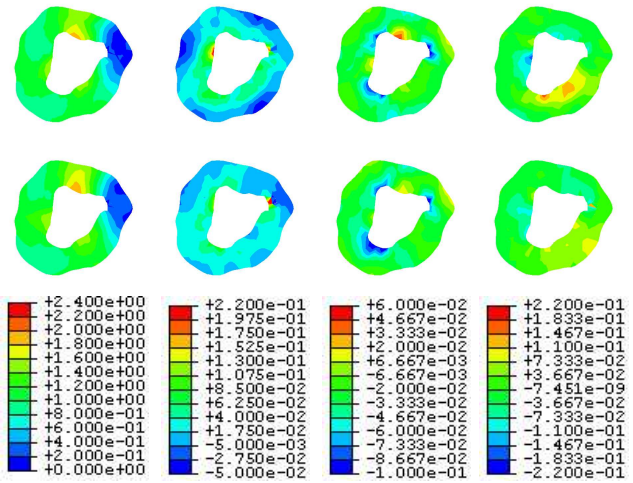

Fig. 3. Left to right: displacement magnitude maps, radial strain maps, circumferential strain maps, and radial-circumferential shear strain maps of frame #9 with respective to frame #1. Top to bottom: with anisotropic material model, with isotropic material model, and the color scales.

3.2. In Vivo Canine MRI Data

Experiments have also been performed using a canine cardiac phase contrast MRI sequence (Fig.1), which measures the instantaneous velocities of the tissues in addition to the typical cardiac anatomy. The heart boundaries and their displacements over the 16-frame cardiac cycle are estimated [16], the myofiber orientations are obtained from the Cardiac Mechanics Research Group at UCSD [2], and the mapping of fiber orientations onto the particular image slice is based on the principal warps algorithm on the landmarks [2]. Boundary displacements and mid-wall phase contrast velocities have been both used in the experiments (Fig. 1).

Fig.3 shows the multiframe-estimated kinematics results using both the anisotropic and isotropic material models. It can be seen that in all cardiac specific strain maps, the strains obtained using anisotropic material model are larger. This is because the Young's modulus along the fiber direction is set to be 3 times larger than that along the cross-fiber direction [5], which means under the same boundary conditions, the deformation along the cross-fiber direction is larger compared with those of the isotropic material. Furthermore, in the radial-circumferential strain maps, the results from anisotropic material model give a considerably better indication of the infarcted myocardium, as validated by the highlighted region of the triphenyl tetrazolium chloride (TTC) stained post mortem mid-ventricle myocardium slice (Fig.1), the clinical gold standard.

4. CONCLUSION

In this paper, we have proposed an nonrigid motion analysis using anisotropic spatial model. The values of using anisotropic material with multiframe strategies have been shown by synthetic experiments, and the algorithm has been tested using MRI cardiac sequence with very promising results.

[2]http://cmrg.ucsd.edu

5. REFERENCES

[1] Y. Bar-Shalom, X.R. Li, and T. Kirubarajan. *Estimation with Applications to Tracking and Navigation*. John Wiley & Sons, Inc., 2001.

[2] F.L. Bookstein. Principal warps: Thin-plate splines and the decomposition of deformations. *IEEE Transactions on Pattern Analysis and Machine Intelligence*, 11:567–585, 1989.

[3] A.J. Frangi, W.J. Niessen, and M.A. Viergever. Three-dimensional modeling for functional analysis of cardiac images: A review. *IEEE Transactions on Medical Imaging*, 20:2–25, 2001.

[4] Y.C. Fung. *Biomechanics : Mechanical Properties of Living Tissues*. Springer-Verlag, 2nd edition, 1993.

[5] L. Glass, P. Hunter, and A. McCulloch, editors. *Theory of Heart : Biomechanics, Biophysics, and Nonlinear Dynamics of Cardiac Function*. Springer-Verlag, 1991.

[6] E.W. Kamen and J.K. Su. *Introduction to Optimal Estimation*. Springer, 1999.

[7] W.S. Kerwin and J.L. Prince. The kriging update model and recursive space-time function estimation. *IEEE Transactions on Signal Processing*, 47:2942–2952, 1999.

[8] H. Liu and P. Shi. Meshfree representation and computation: applications to cardiac motion analysis. In *Information Processing in Medical Imaging*, pages 560–572, 2003.

[9] E.W.B. Lo, H. Liu, and P. Shi. H_∞ filtering and physical modeling for robust kinematics estimation. In *IEEE International Conference on Image Processing*, pages 169–172, 2003.

[10] F.L. Matthews and R.D. Rawlings. *Composite Materials: Engineering and Science*. Chapman & Hall, 1994.

[11] J.C. McEachen and J.S. Duncan. Multiframe temporal estimation of cardiac nonrigid motion. *IEEE Transactions on Medical Imaging*, 16:270–283, 1997.

[12] P.M.F. Nielson, I.J. LeGrice, B.H. Smaill, and P.J. Hunter. Mathematical model of geometry and fibrous structure of the heart. *American Journal of Physiology*, 260:H1365–H1378, 1991.

[13] X. Papademetris, A.J. Sinusas, D.P. Dione, R.T. Constable, and J.S. Duncan. Estimation of 3D left ventricular deformation from medical images using biomechanical models. *IEEE Transactions on Medical Imaging*, 21:786–799, 2002.

[14] P. Shi, A. Sinusas, R.T. Constable, and J. Duncan. Volumetric deformation analysis using mechanics-based data fusion: Applications in cardiac motion recovery. *International Journal of Computer Vision*, 35:87–107, 1999.

[15] C.L. Wong, H. Liu, L.N. Wong, A.J. Sinusas, and P. Shi. Meshfree cardiac motion analysis framework using composite material model and total Lagrangian formulation. In *IEEE International Symposium on Biomedical Imaging: Macro to Nano*, pages 464–467, 2004.

[16] L.N. Wong, H. Liu, A. Sinusas, and P. Shi. Spatio-temporal active region model for simultaneous segmentation and motion estimation of the whole heart. In *IEEE Workshop on Variational, Geometric and Level Set Methods in Computer Vision*, pages 193–200, 2003.